

Supplementary Information

Additional text

Polyols and monosaccharides concentrations

Mannitol was quantified on June 16, 22, and 26, and September 11, when average daily RH and temperature were above 75% and 18 °C, respectively (Figure S1). Arabitol was detected on June 26, and September 04, 10, and 11. Its frequency increased after the occurrence of rain in September (days 01 to 03), followed by higher temperatures after day 09, marking the transition to spring.

Levoglucosan represented 3.3% of OM (from 0.6 to 7.8%). A similar share (3.1%) was observed in the 2014 dry period.

Meteorological data and fire outbreaks

During the four-month period (June-September), the monthly average temperature and humidity fell below the climatological mean (CM), registering 16.9 °C (CM: 17.5 °C) and 71.7% (CM: 80.4%), respectively, as reported in the annual meteorological bulletin by the climatological station of IAG-USP for 2019 (IAG-USP, 2023). The monthly average accumulated precipitation was 54.2 mm, with a mean deviation (MD) of 64.8 mm. The distribution of precipitation throughout the period was notably irregular, primarily characterized by a singular event of heavy rainfall on July 04, which set an absolute record for July in the climatological series with 115 mm. Only four other days recorded precipitation exceeding 10 mm, on July 05, September 01, 02, and 03, which amounted to 26, 35, 17, and 21 mm, respectively. Multiple incursions of cold fronts occurred in the Brazilian territory during the period, predominantly affecting the southern region of the country. Specifically in São Paulo city, six fronts reached the area on June 04 and 20, and on August 02, 13, 18, and 31. Conditions of hot and dry air masses and high subtropical pressure and atmospheric stability resulted in high PM_{2.5} events in several cities in the state of São Paulo, between June 11 and 16, July 10 and 15, and one outside the sampling campaign, between September 15 and 20 (CETESB, 2020). Between June and September, the number of fires registered in the country increased from 7258 to 53234 (INPE, 2024). Almost all Brazilian states registered fires, however, the Center-Western state of Mato Grosso presented the highest numbers in June, July, and September, and the Northern state of Pará, in August.

Comparison with other studies

Some countries in South America follow stricter daily PM_{2.5} limits than Brazil, such as Colombia, Chile, and Ecuador (between 37.5 and 50 $\mu\text{g m}^{-3}$), while Argentina and Peru lack standards for this pollutant. The US National Ambient Air Quality Standards (NAAQS) recommended a decrease in the 24 h PM_{2.5} limit from 65 $\mu\text{g m}^{-3}$ to 35 $\mu\text{g m}^{-3}$ in 2006 (Cheng et al., 2023).

In another study performed in São Paulo (2019-2020), but in a site in the eastern region of the city and nearer the ocean, organic matter (OM) corresponded to a similar fraction of over 41% of PM_{2.5} (26% of PM_{2.5} if considering OC) (Vieira et al., 2023). If previous studies are taken into account, a reduction in the proportion of EC and an increase in OM was observed, since EC represented 16% and 14% and OM 36% and 34%, in the 2014 and 2008 intensive campaigns, respectively (Pereira et al., 2017b; Souza et al., 2014) (Table S2). Cheng et al. (2023) also observed an increase in the carbonaceous fraction (OM + EC) in the last decades in several US cities, while a decline in EC due to emission control measures was experienced in other metropolises around the world, such as Hong Kong, China (Chow et al., 2022) and Nagoya, Japan (Yamagami et al., 2019).

A reduction was also observed in the period between 2007-2017 in Hong Kong as a result of the control of SO₂ emissions from industries and vehicles (Chow et al., 2022). Between 2006 and 2020, the contribution of inorganic species such as NH₄⁺, NO₃⁻ and SO₄²⁻ decreased in the USA (Cheng et al., 2023), contributing to the reduction in PM_{2.5} levels. Furthermore, many metropolises in South America have experienced a decrease in sulfur dioxide levels (Gómez Peláez et al., 2020). Earlier before, in the 1990s, a decrease in SO₄²⁻ was observed in different European countries (1991-2001), although the same was not observed for NO₃⁻ (Chow et al., 2022; Putaud et al., 2004). In Europe, emission and fuel control measures were adopted earlier.

In Brazil, since 2013, the S10 diesel (10 ppm of sulfur) substituted the S50 diesel (50 ppm), whereas in 2014 the S50 gasoline replaced the S800 gasoline (800 ppm), although older trucks are still allowed to use S500 (500 ppm) diesel (CETESB, 2015).

Figures

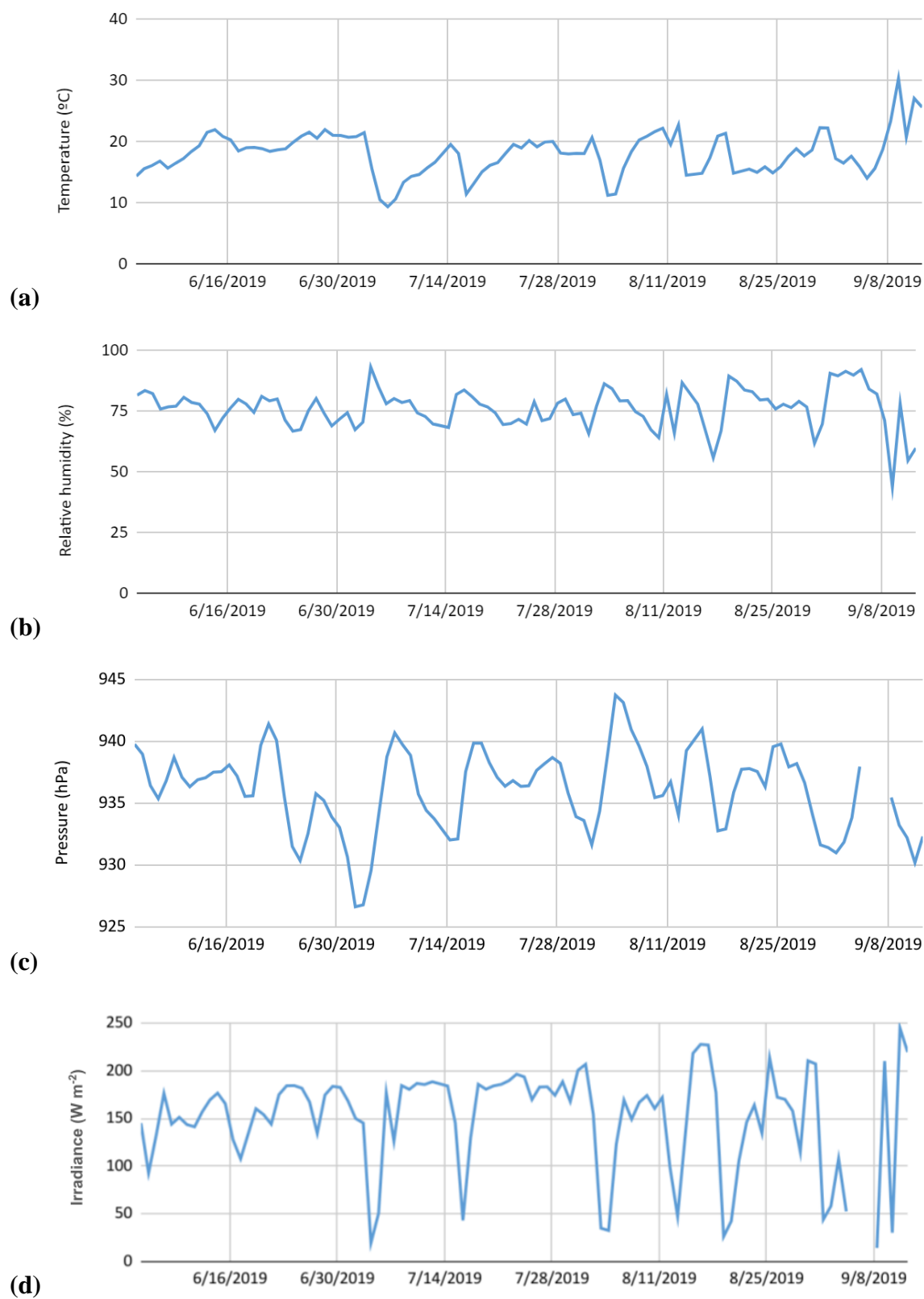


Figure S1. Meteorological conditions during the sampling campaign: average daily temperature **(a)**, relative humidity **(b)**, pressure **(c)**, and irradiance **(d)**.

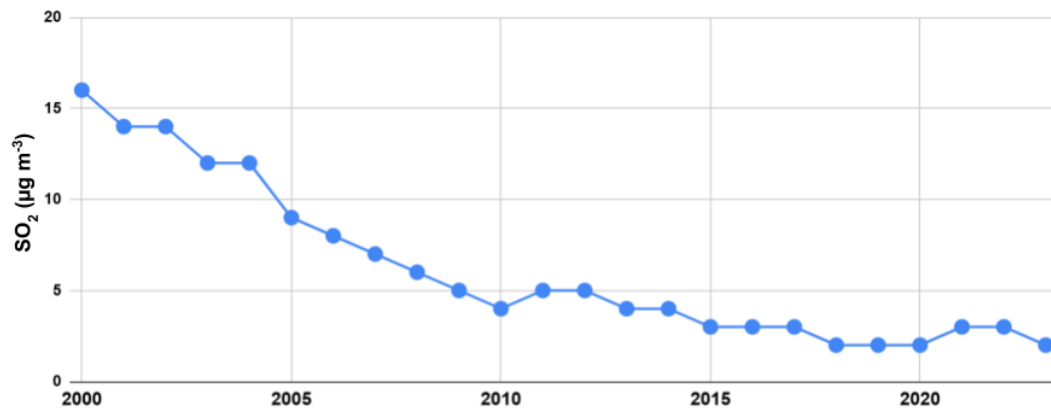


Figure S2. Yearly evolution of SO_2 concentrations in the MASP. Adapted from CETESB (2020).

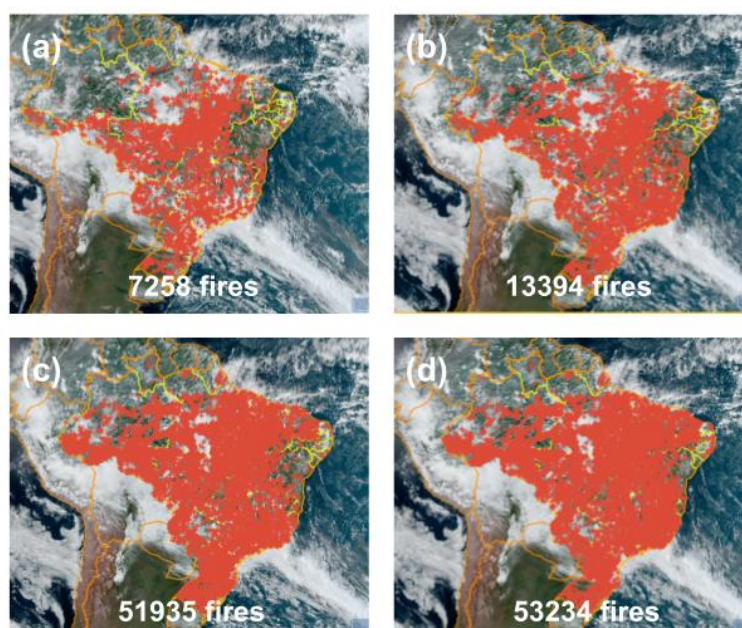


Figure S3. Fires registered by satellite in June (a), July (b), August (c), and September (d). Data was collected by the MODIS instrument on Aqua satellite (INPE, 2019).

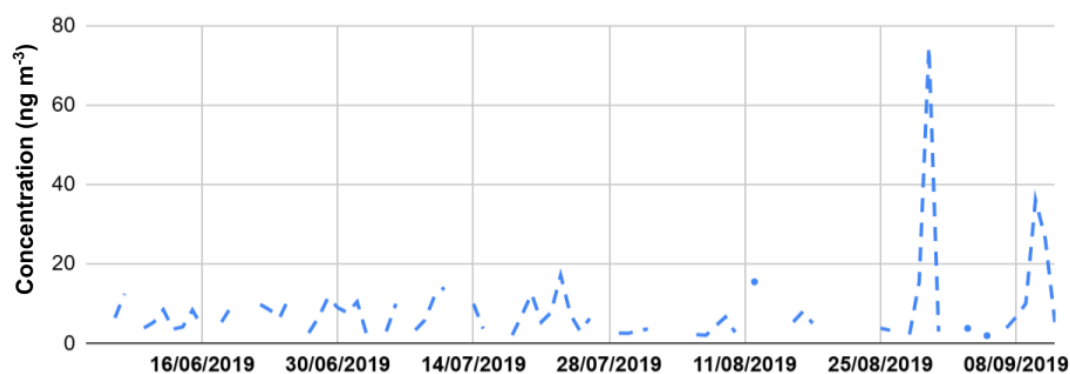


Figure S4: Daily series for xylitol concentrations (ng m^{-3}).

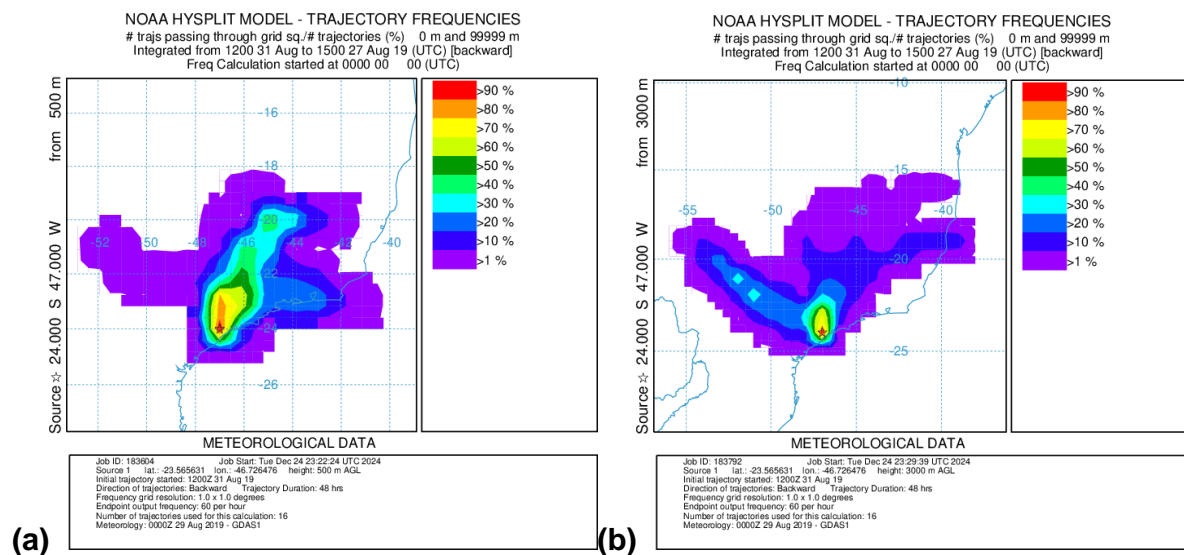


Figure S5: Backward trajectory frequencies for August 29 and 30, 2019, arriving at 500 m (a) and 3000 m (b).

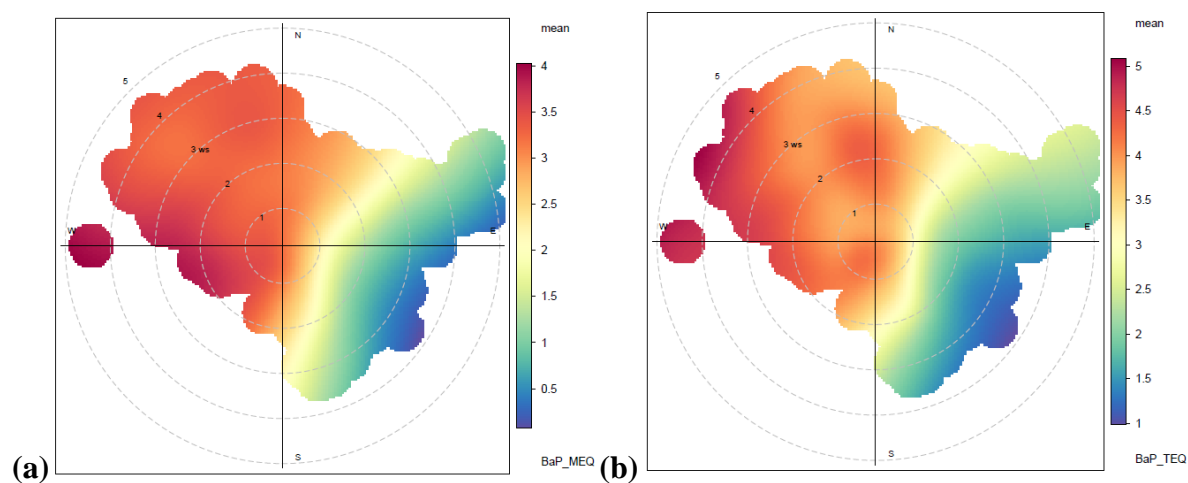


Figure S6: Polar plots for benzo(a)pyrene mutagenicity (a) and toxicity (b) equivalent indexes.

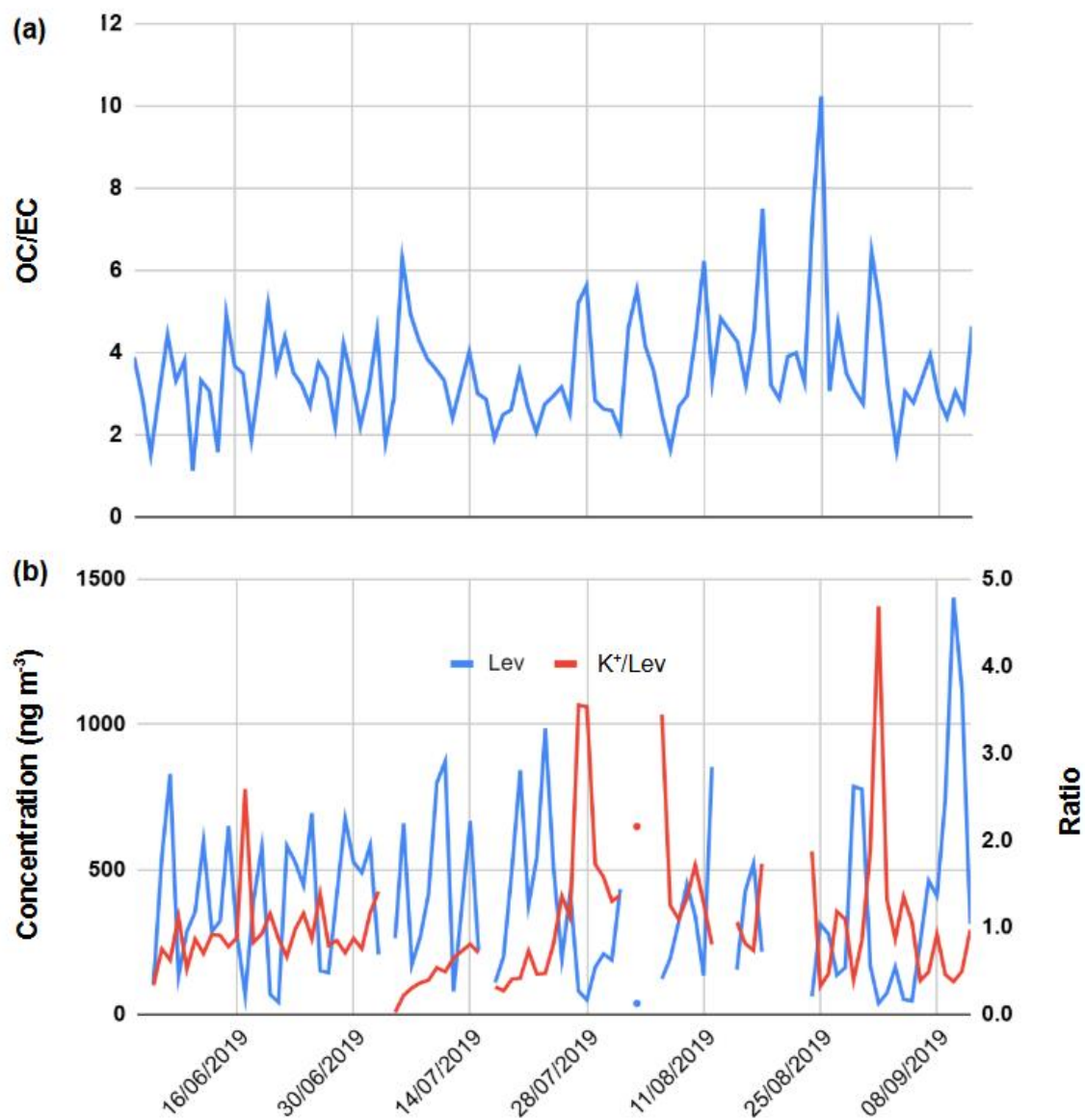


Figure S7: Daily OC/EC ratios (a), levoglucosan concentrations (ng m⁻³) and K⁺/Lev ratios throughout the campaign (b).

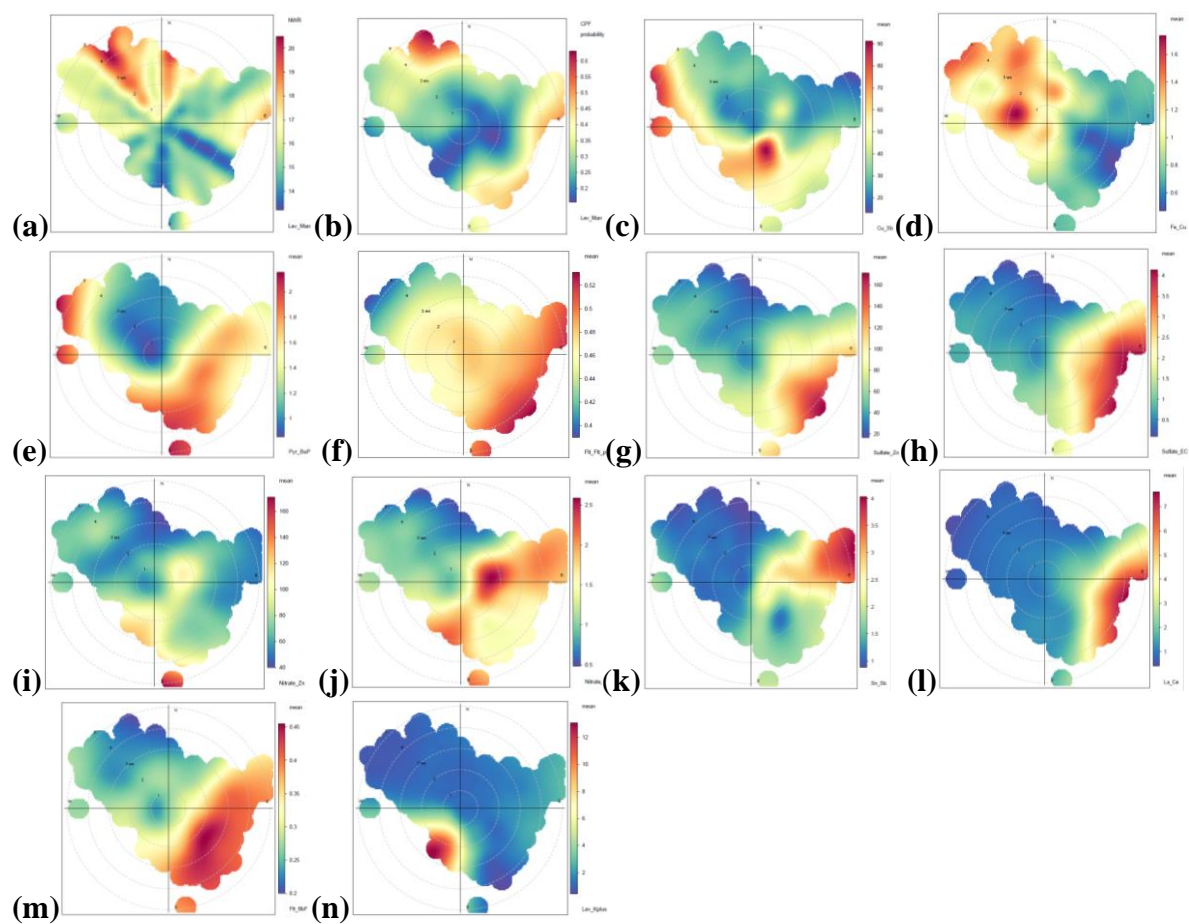


Figure S8:. Polar plots for Lev/Man (a) (NWR), and Lev/Man (b) (CPF), Cu/Sb (c), Fe/Cu (d), Pyr/BaP (e), Flt/(Flt+Pyr) (f), $\text{SO}_4^{2-}/\text{Zn}$ (g), $\text{SO}_4^{2-}/\text{EC}$ (h), NO_3^-/Zn (i), NO_3^-/EC (j), Sn/Sb (k), La/Ce (l), Flt/BbF (m), Lev/ K^+ (n) (mean).

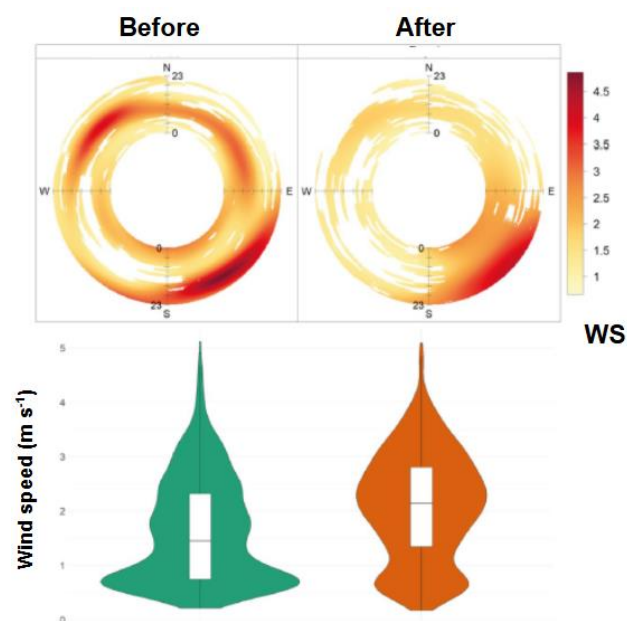
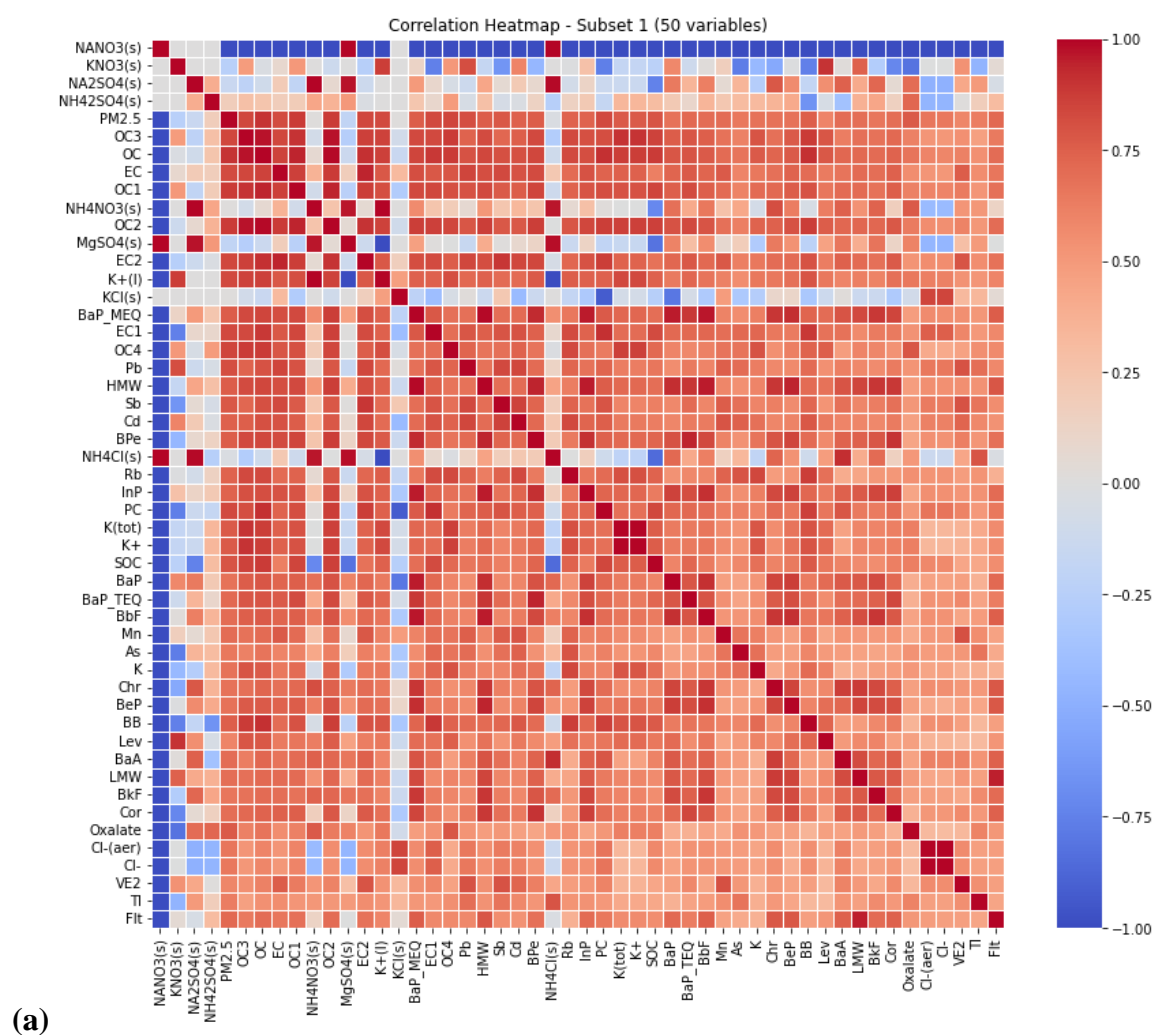
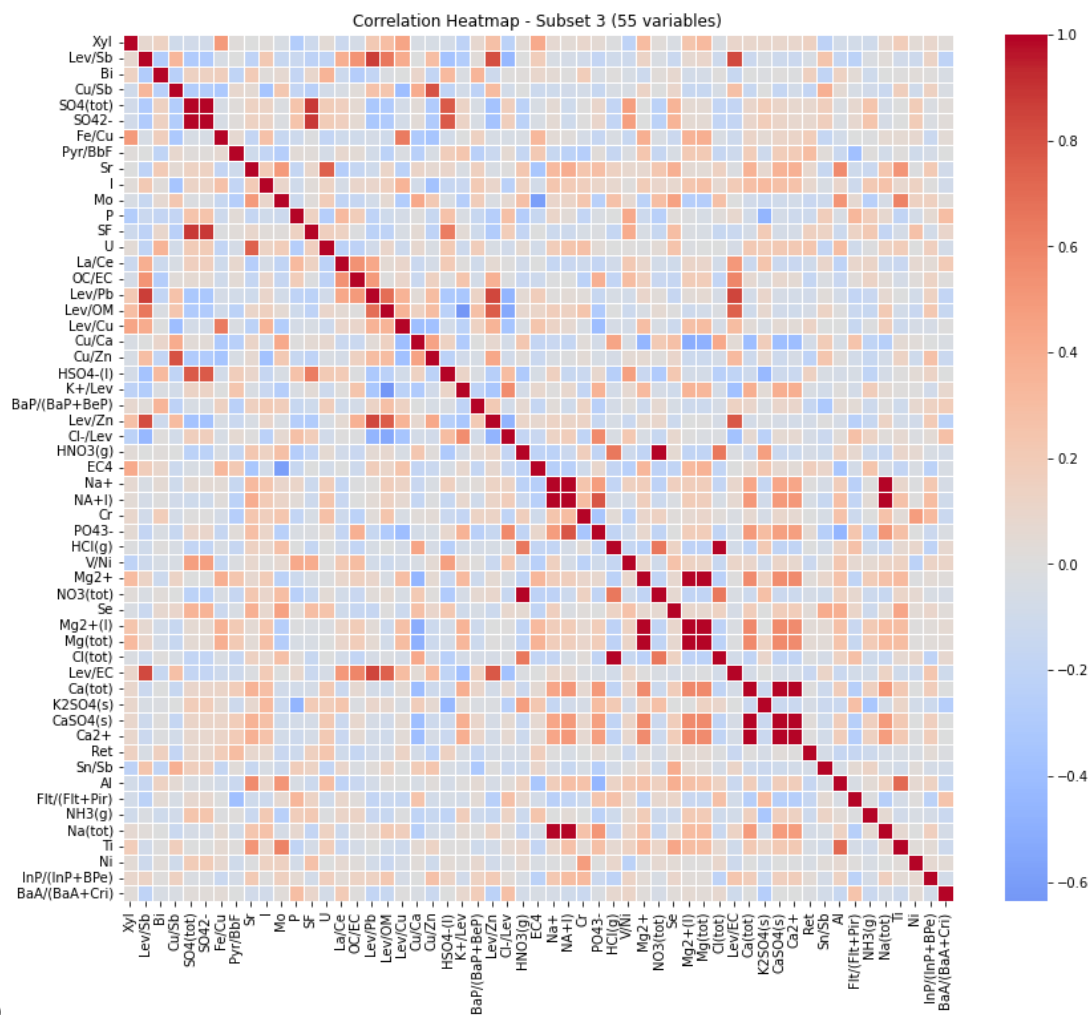


Figure S9: Hourly annulus plot for wind frequency and wind speed distribution, before and after the beginning of August, adapted from Kamigauti (2024).





(b)

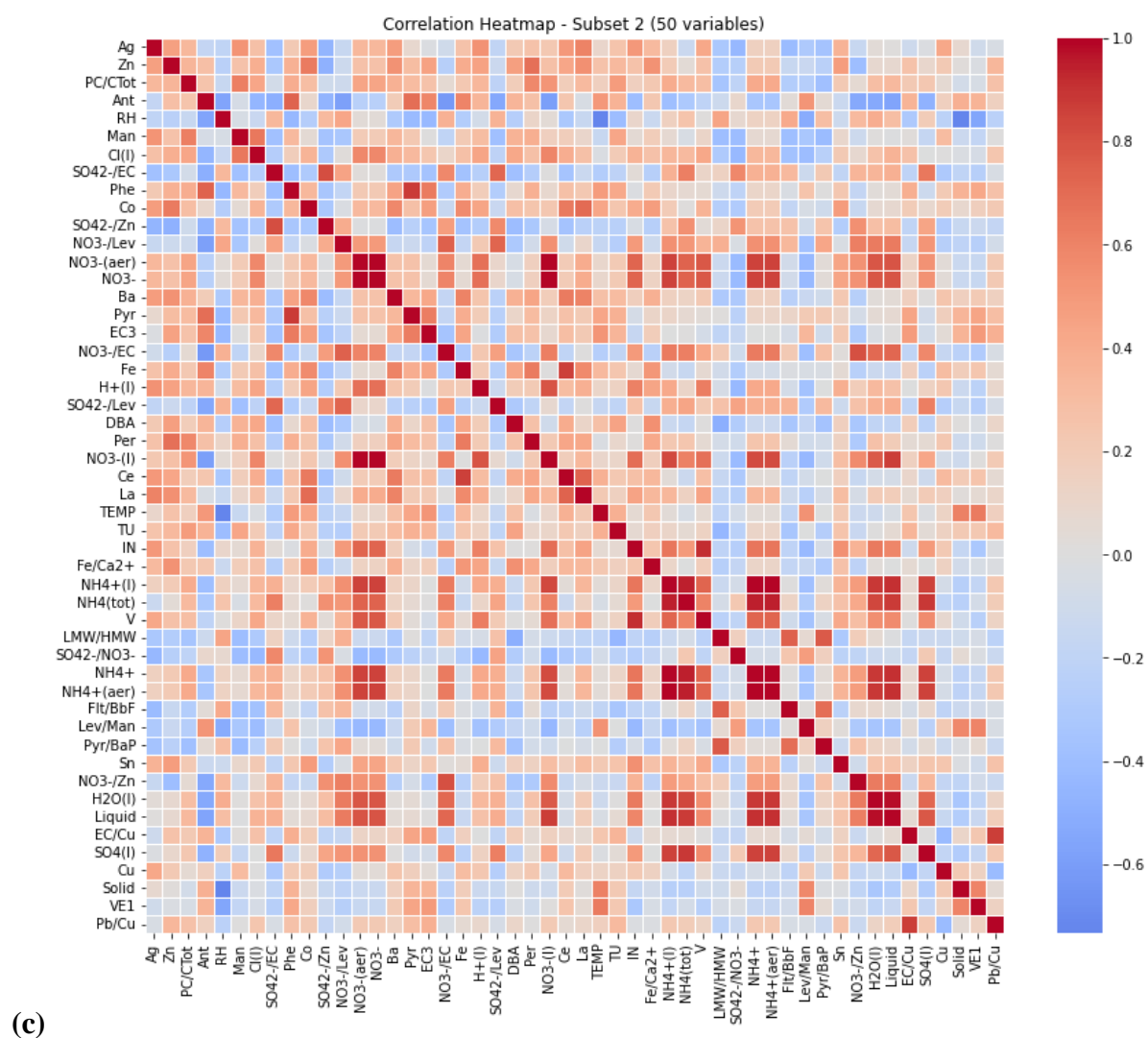


Figure S10: Pearson correlation heatmap subset 1 (a), 2 (b) and 3 (c).

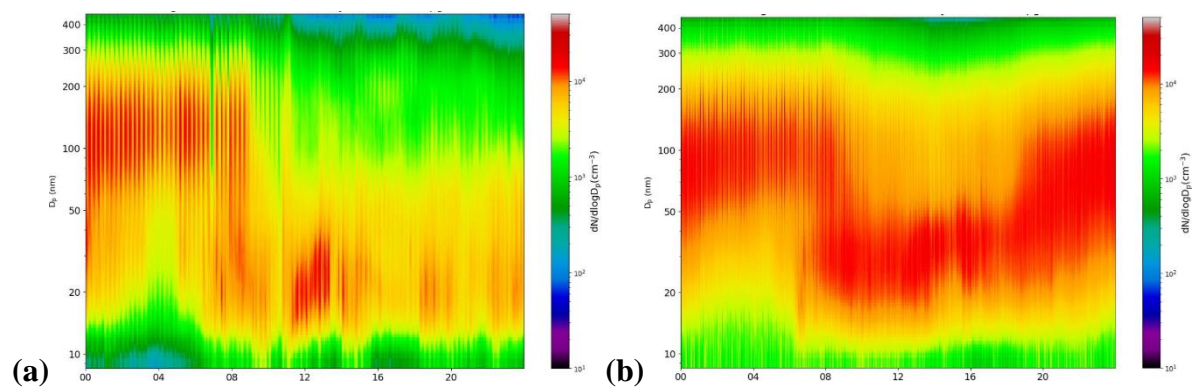


Figure S11: Average submicrometer particle number size distributions for (a) clean and ($\text{PM}_{2.5} < 15 \mu\text{g m}^{-3}$) (b) polluted periods ($\text{PM}_{2.5} \geq 15 \mu\text{g m}^{-3}$).

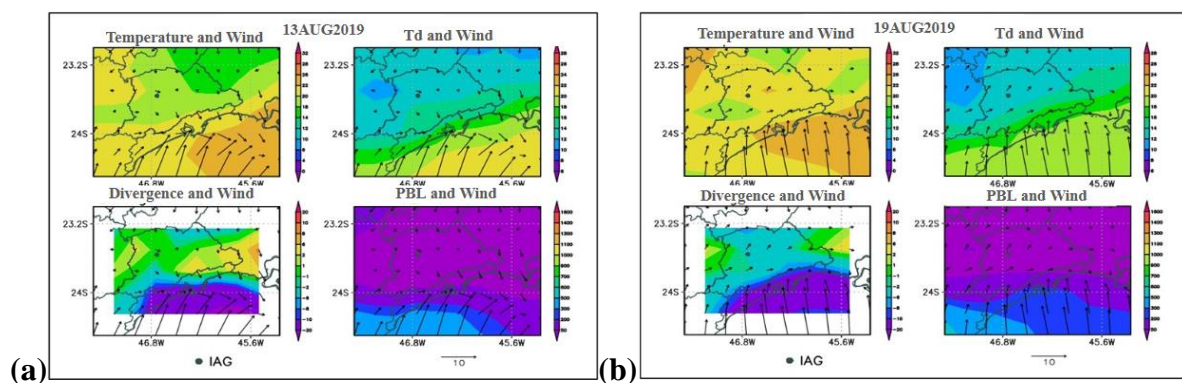


Figure S12: Air masses and meteorological conditions on August 13 (a) and 19 (b) obtained with Grid Analysis and Display System (GrADS).

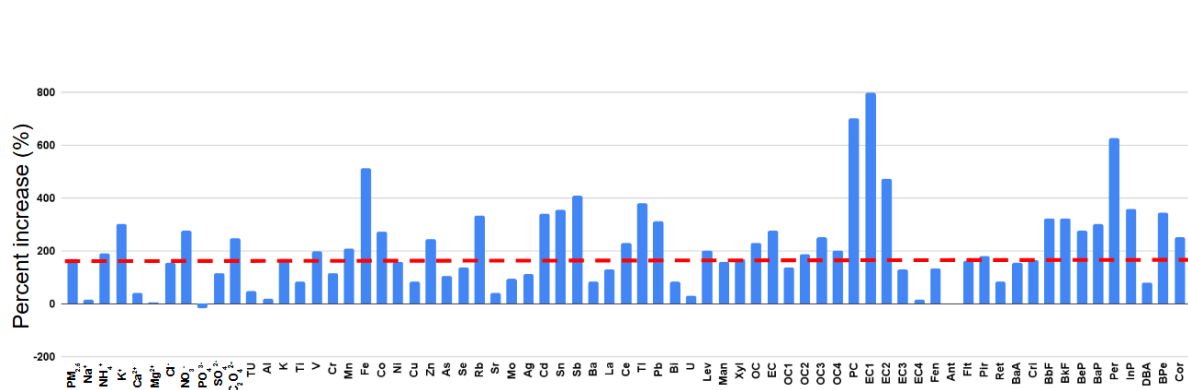


Figure S13: Relative increase of chemical species during PM_{2.5} pollution events. PM_{2.5} is marked by the dotted line.

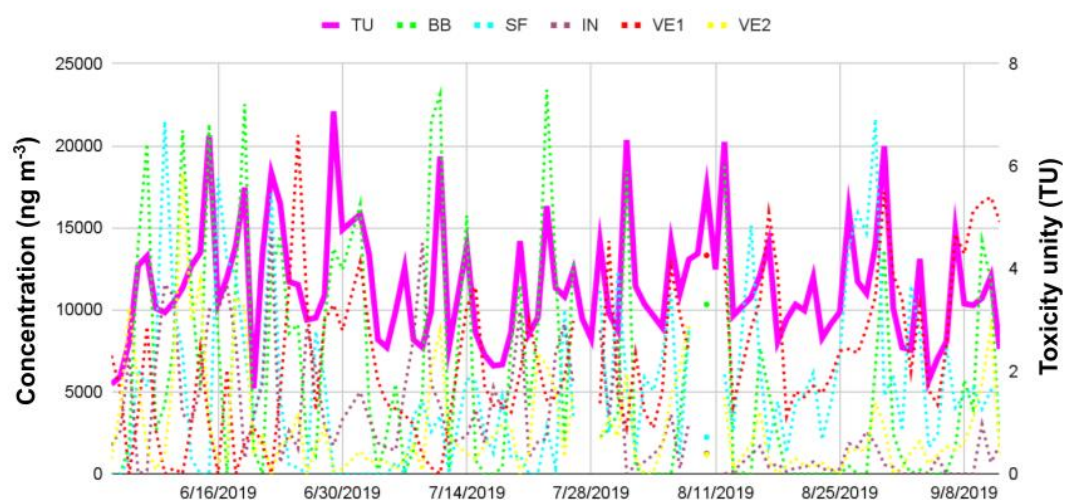


Figure S14: PMF factor concentrations and toxicity units (TU).

Tables

Table S1. Analytical parameters: retention time (RT), limit of detection (LOD), limit of quantification (LOQ), recoveries for each PAH, mean recovery and standard deviation.

PAH	Abbrev.	m/z	RT	LOD	LOQ	Rec.
			(min)	(ng mL ⁻¹)	(ng mL ⁻¹)	(%)
Phenanthrene	Phe	178	14.475	2.5	7.5	48.9
Anthracene	Ant	178	14.668	2.5	7.5	50.8
Fluoranthene	Flt	202	18.060	1.25	3.75	96.7
Pyrene	Pyr	202	18.715	1.25	3.75	98.6
Retene	Ret	219	19.897	5	15	108.6
Benzo(a)anthracene	BaA	228	23.878	5	15	100.4
Chrysene	Chr	228	23.949	5	15	119.6
Benzo(b)fluoranthene	BbF	252	30.202	10	30	131.2
Benzo(k)fluoranthene	BkF	252	20.239	7.5	22.5	136.4
Benzo(e)pyrene	BeP	252	31.906	7.5	22.5	137.2
Benzo(a)pyrene	BaP	252	31.959	10	30	98.7
Perylene	Per	252	32.022	10	30	82.1
Indeno(1,2,3-cd)pyrene	InP	276	39.979	10	30	99.9
Dibenzo(a,h)anthracene	DBA	278	40.469	10	30	82.2
Benzo(g,h,i)perylene	BPe	276	41.595	10	30	102.2
Coronene	Cor	300	51.662	10	30	110.0
Mean						100.2
SD						25.4
				(µg mL ⁻¹)	(µg mL ⁻¹)	
Fluoride	-	-	-	0.01	0.04	82
Formiate	-	-	-	0.01	0.03	85
Chloride	-	-	-	0.03	0.08	90
Nitrate	-	-	-	0.01	0.03	112
Sulfate	-	-	-	0.01	0.04	100
Oxalate	-	-	-	0.01	0.04	90
Sodium	-	-	-	0.02	0.07	81
Ammonium	-	-	-	0.03	0.10	84
Potassium	-	-	-	0.02	0.06	91
Calcium	-	-	-	0.04	0.12	89
Magnesium	-	-	-	0.05	0.15	104
Mean						92
SD						9
				(µg cm ⁻²)	(µg cm ⁻²)	
OC	-	-	-	0.4	1.2	-
EC	-	-	-	0.2	0.6	-

Table S2. Percent of abundant chemical species in particulate matter (OM, EC, SO₄²⁻, and NO₃⁻) in previous studies in this sampling site.

Year	2008	2010	2013	2014		2019			
Ref.	Souza et al. (2014)	Pereira et al. (2019)	Pereira et al. (2017a)	Pereira et al. (2017b)		Present study			
Size	PM _{2.5}	PM ₁₀	PM ₁₀	PM _{2.5}	PM _{2.5}	PM _{2.5}			
Season	Winter	Winter	Winter	Winter	All	Fall	Winter		
Month	Aug	Jun	Jul/Aug	Jul	Jan-Sep	Jun	Jul	Aug	Sep
N	22	12	11	12	32	27	30	30	12
SO₄²⁻	7	4	5	7	11	8	8	8	7
NO₃⁻	4	4	3	6	5	11	13	8	8
OM	35	22	19	36	36	48	49	44	47
EC	14	10	10	16	13	10	10	8	10
Other	40	60	63	35	36	23	21	32	28

Table S3. Median, average, minimum and maximum values for PAH diagnostic ratios.

(ng m ⁻³)	Med.	Ave.	Min.	Max.
Phe	0.22	0.28	0.03	0.87
Ant	0.07	0.07	0.03	0.12
Flt	0.38	0.49	0.06	1.65
Pyr	0.44	0.54	0.07	1.96
Ret	0.22	0.33	0.05	1.49
BaA	0.34	0.43	0.07	1.79
Chr	0.55	0.68	0.07	2.65
BbF	1.36	1.8	0.13	8.56
BkF	0.47	0.62	0.01	2.2
BeP	1	1.34	0.07	5.49
BaP	0.54	0.64	0.04	2.39
Per	0.27	0.33	0.05	1.06
InP	0.73	1.15	0.15	4.65
DBA	0.29	0.39	0.09	1.46
BPe	0.86	1.27	0.11	4.55
Cor	0.31	0.47	0.05	2.03
ΣPAHs	7.46	10.08	1.08	37.35
BaP_TEQ	0.94	1.91	0.06	8.64
BaP_MEQ	1.12	1.73	0.16	7.29
BaPE	0.57	0.92	0.04	4.08
BaP/(BaP+BeP)	-	0.32	0.11	0.45
Flt/(Flt+Pir)	-	0.48	0.32	0.72
InP/(InP+BPe)	-	0.48	0.28	0.65
BaA/(BaA+Cri)	-	0.38	0.19	0.64
LMW/HMW	-	0.35	0.1	1.12
Pyr/BaP	-	0.85	0.17	4.59
Pyr/BbF	-	0.3	0.07	1.39
Flt/BbF	-	0.27	0.08	0.95

Table S4. Correlation matrix for the dataset is in the **zipped attached file**.

Table S5. Percentage distribution of particles in different modes (nucleation, Aitken and accumulation).

%	Nucleation	Aitken	Accumulation
Ave.	21	46	32
Min.	0	21	12
Max.	48	73	68

Table S6. Average species' concentrations in non-polluted ($\text{PM}_{2.5} < 15 \mu\text{g m}^{-3}$) and polluted ($\text{PM}_{2.5} \geq 15 \mu\text{g m}^{-3}$) periods.

	Non-polluted	Polluted		Non-polluted	Polluted
($\mu\text{g m}^{-3}$)			(ng m^{-3})		
$\text{PM}_{2.5}$	10.7	29.1	Cr	1.81	3.92
OC	2.6	8.7	Mn	2.70	8.40
EC	0.8	2.9	Fe	18.00	110.00
OC1	0.7	1.5	Co	0.03	0.10
OC2	0.7	2.1	Ni	0.94	2.42
OC3	0.4	1.5	Cu	83.00	153.30
OC4	0.7	2.0	Zn	17.40	59.80
PC	0.1	1.4	As	0.70	1.40
EC1	0.2	1.7	Se	0.71	1.67
EC2	0.3	1.7	Rb	0.63	2.74
EC3	0.4	0.8	Sr	4.04	5.66
EC4	0.1	0.1	Mo	2.89	5.58
(ng m^{-3})			Ag	0.14	0.29
Na^+	148.64	172.90	Cd	0.18	0.82
NH_4^+	393.62	1143.26	Sn	2.20	10.20
K^+	82.14	330.44	Sb	1.40	7.20
Ca^+	98.01	137.44	Ba	10.08	18.36
Mg^{2+}	41.72	43.79	La	0.15	0.34
Cl^-	147.64	375.69	Ce	0.10	0.31
NO_3^-	827.40	3107.05	Tl	0.02	0.08
PO_4^{3-}	359.72	304.16	Pb	4.10	16.70
SO_4^{2-}	1033.38	2249.48	Bi	0.12	0.22
$\text{C}_2\text{O}_4^{2-}$	53.15	185.63	U	0.20	0.26
Al	178.00	214.00	Lev	140.03	423.00
K	127.00	339.00	Man	11.92	31.00
Ti	5.50	10.00	Xyl	3.26	8.76
V	0.70	2.10			

OC1 is the most volatile fraction of organic carbon and is strongly correlated with species from both biomass burning and vehicular sources, such as K^+ and some elements (Mn, Cd, Sb, and Pb) (Table S5). Most OC and EC fractions presented correlations with each other, except for EC3 and EC4. The fraction EC4 correlated with EC3, but not with other species. Both were more associated with VE1. EC3 was previously assigned to HDV emissions (Pereira et al., 2023a). In former studies conducted in São Paulo, it was observed that OC3 and OC4 presented strong correlations with each other, as well as with EC. This was attributed to well-processed primary vehicular emissions or secondarily formed aerosols from anthropogenic gaseous precursors (Monteiro dos Santos et al., 2016). Secondary organic carbon (SOC) was estimated considering the 5th percentile of the OC/EC ratios (Monteiro dos Santos et al., 2016) and its contribution reached nearly half of OC, reaching a maximum of 83%. Among the OC and EC fractions, SOC was more correlated with PC (Table S5). This OC fraction has been previously attributed to water-soluble organic carbon (WSOC), sometimes used as a proxy for SOC (Monteiro dos Santos et al., 2016). In the 2018 tunnel study, PC increased with increasing HDV emissions, suggesting an association with biodiesel (Pereira et al., 2023b). However, it can also be apportioned to biomass burning. Correlations with BB were higher for the OC2 and OC3 fractions. Among the elemental carbon fractions, EC1 presented a higher correlation with BB, and EC2 with VE2. Concerning specific organic species, OC2 displayed higher correlations with PAHs, increasing for HMW-PAH, while levoglucosan showed higher correlations with OC3.

Temperature correlated moderately with $PM_{2.5}$, K^+ , oxalate, OC, EC, VE1, Lev/Man ratio, $K_2SO_{4(s)}$, Relative humidity (RH) presented moderate negative correlations with $PM_{2.5}$, K^+ , oxalate, Rb, OC, BaP-MEQ, VE1, and Lev/Man ratio, weak positive relationships with the ratios LMW/HMW, Flt/BbF, NO_3^-/EC , SO_4^{2-}/EC , SO_4^{2-}/Zn , and NO_3^-/Zn , and moderate positive dependences on modeled liquid aerosol and water content. Cloudier and cooler conditions, associated with higher RH, may favor the amounts of LMW-PAHs in relation to HMW-PAHs and enhance the formation of secondary inorganic species. Irradiation presented weak correlations with most species, but higher with K^+ , and, as expected, was also associated with higher temperatures. BaP/(BaP+BeP) was not correlated with radiation. However, a negative correlation with the LMW-PAHs/HMW-PAHs ratio was observed. Although with a weak Pearson coefficient, atmospheric pressure was negatively correlated with K^+ , Rb, Ce, Lev, OC and EC. Inverse moderate correlation were also established between atmospheric pressure and VE1, modeled solid aerosol. Weak positive interrelationships were obtained with

the La/Ce, V/Ni, $\text{SO}_4^{2-}/\text{NO}_3^-$, $\text{SO}_4^{2-}/\text{EC}$ ratios, suggesting an increase in sulfate formation under increased atmospheric pressure. The OC/EC ratio showcased inverse weak correlations with the primary vehicular-related tracers Zn and Pb ($r \leq -0.4$). This ratio tends to be lower in HDV primary emissions (Pereira et al., 2023a).

References

- CETESB: Companhia de Tecnologia do Saneamento Ambiental: Relatório de qualidade do ar no Estado de São Paulo 2014, Report of air quality in the São Paulo State 2014, São Paulo, Brazil, available at: <http://ar.cetesb.sp.gov.br/publicacoes-relatorios/> (last access: 1 February 2024), 2015.
- Cheng, B., Alapaty, K. and Arunachalam, S.: Spatiotemporal trends in $\text{PM}_{2.5}$ chemical composition in the conterminous U.S. during 2006–2020, *Atmos. Environ.*, 120188, <https://doi.org/10.1016/j.atmosenv.2023.120188>, 2023.
- Chow, W. S., Liao, K., Huang, X. H. H., Leung, K. F., Lau, A. K. H. and Yu, J. Z.: Measurement report: The 10-year trend of $\text{PM}_{2.5}$ major components and source tracers from 2008 to 2017 in an urban site of Hong Kong, China, *Atmospheric Chemistry and Physics*, 22(17), 11557–11577, <https://doi.org/10.5194/acp-22-11557-2022>, 2022a.
- Gómez Peláez, L. M., Santos, J. M., de Almeida Albuquerque, T. T., Reis, N. C., Andreão, W. L. and de Fátima Andrade, M.: Air quality status and trends over large cities in South America, *Environmental Science & Policy*, 114, 422–435, <https://doi.org/10.1016/j.envsci.2020.09.009>, 2020.
- Kamigauti, L.Y.: Environmental magnetism applied on the largest metropolis in Latino America: vehicular fleet, emission sources, and new technologies, Ph.D. thesis, Institute of Astronomy, Geophysics, and Atmospheric Sciences, University of São Paulo, 2024.
- Monteiro dos Santos, D. A., Brito, J. F., Godoy, J. M. and Artaxo, P.: Ambient concentrations and insights on organic and elemental carbon dynamics in São Paulo, Brazil, *Atmos. Environ.*, 144, 226–233, <https://doi.org/10.1016/j.atmosenv.2016.08.081>, 2016.
- Pereira, G. M., Nogueira, T., Kamigauti, L. Y., Monteiro Dos Santos, D., Nascimento, E. Q. M., Martins, J. V., Vicente, A., Artaxo, P., Alves, C., de Castro Vasconcellos, P. and de Fatima Andrade, M.: Particulate matter fingerprints in biofuel impacted tunnels in South America's largest metropolitan area., *Sci. Total Environ.*, 856(Pt 2), 159006, <https://doi.org/10.1016/j.scitotenv.2022.159006>, 2023b.
- Putaud, J.-P., Raes, F., Van Dingenen, R., Brüggemann, E., Facchini, M.-C., Decesari, S., Fuzzi, S., Gehrig, R., Hüglin, C., Laj, P., Lorbeer, G., Maenhaut, W., Mihalopoulos, N., Müller, K., Querol, X., Rodriguez, S., Schneider, J., Spindler, G., Brink, H. ten, Tørseth, K. and Wiedensohler, A.: A European aerosol phenomenology—2: chemical characteristics of particulate matter at kerbside, urban, rural and background sites in Europe, *Atmos. Environ.*, 38(16), 2579–2595, <https://doi.org/10.1016/j.atmosenv.2004.01.041>, 2004.
- Vieira, E. V. R., do Rosario, N. E., Yamasoe, M. A., Morais, F. G., Martinez, P. J. P., Landulfo,

E. and Maura de Miranda, R.: Chemical characterization and optical properties of the aerosol in São Paulo, Brazil, *Atmosphere*, 14(9), 1460, <https://doi.org/10.3390/atmos14091460>, 2023.

Yamagami, M., Ikemori, F., Nakashima, H., Hisatsune, K. and Osada, K.: Decreasing trend of elemental carbon concentration with changes in major sources at Mega city Nagoya, Central Japan, *Atmos. Environ.*, 199, 155–163, <https://doi.org/10.1016/j.atmosenv.2018.11.014>, 2019.